

# Using NRG to solve quantum impurity models for heavy-fermion systems

Bryan Daniels, Ohio Wesleyan University  
with Kevin Ingersent, University of Florida

July 29, 2004

## Abstract

Computer programs applying the numerical renormalization group (NRG) method to the Kondo and spin-boson models were used to determine the physical properties of heavy-fermion systems. In the first part of the project,  $C$  (specific heat) vs.  $T$  (temperature) plots were created for the Kondo impurity model with an external magnetic field. These plots were compared with previously gathered experimental data for  $\text{Ce}_{0.6}\text{La}_{0.4}\text{Pb}_3$ , a heavy-fermion system. After fitting one unknown parameter, the numerical results were found to reproduce well the field dependence of the temperature and height of the low-temperature peak in  $C$ . The second part of the project involved the quantum critical point of the spin-boson model. A method was developed for automatically finding the critical coupling using the NRG programs. Once located, the critical point was studied numerically. Specifically, critical exponents were found for  $T^*$ , the crossover temperature from the critical regime to the weak- and strong-coupling regimes of the model.

# 1 Introduction

When magnetic impurity atoms are introduced into a metal, at low temperatures the electrical resistance increases as the temperature is lowered, contrary to the normal dependence. This so-called “Kondo effect” is due to conduction electrons scattering with the impurity atoms; this scattering creates an effective force between the electrons, increasing, for example, their effective mass. Materials with dense arrangements of magnetic atoms exhibit similar behavior, and are referred to as “heavy-fermion” systems.

My project consisted of two parts; in the first, I used numerical renormalization group (NRG) programs for the Kondo model of a magnetic impurity in a metal to calculate the specific heat versus temperature in various applied magnetic fields. The resulting curves were compared with previously gathered experimental data for the heavy-fermion system  $\text{Ce}_{0.6}\text{La}_{0.4}\text{Pb}_3$ . The agreement of the numerical and experimental curves suggests that single-impurity physics dominates in  $\text{Ce}_{0.6}\text{La}_{0.4}\text{Pb}_3$ , and that the interactions between the magnetic (Ce) atoms are relatively unimportant. The second part of my project dealt with quantum (zero temperature) phase transitions in the spin-boson model (a simplified version of a model that can be applied to explain some properties of heavy-fermion materials). I worked on extending the NRG method for use with such impurity problems as the spin-boson model, where bosonic degrees of freedom are included. This work should lead to a better understanding of the low-temperature behavior of heavy-fermion systems.

## 2 Background

### 2.1 The Kondo and Spin-Boson Models

The two models used in my project were the Kondo impurity model and the spin-boson model. These are both quantum impurity models, which attempt to describe the behavior of a large system with some number of magnetic impurities by focusing on a single impurity atom’s spin and the material that surrounds it. There is an important difference between the two types of models we used: In the Kondo model, the impurity spin

interacts with fermions (for instance, the conduction electrons in a metal), while in the spin-boson model the impurity couples to bosons (representing, for example, vibrations in the atomic lattice). In both models, the impurity is assumed to have spin  $S = 1/2$ .

These single-impurity models represent a huge simplification from the complexities present in a heavy-fermion material, which has a dense arrangement of magnetic atoms. They implicitly assume, for example, that there is no interaction between the magnetic atoms, so that the properties of the system simply scale linearly with the number of impurity atoms.

Each of these models is defined using a quantum-mechanical Hamiltonian, a way of describing the total energy of a system. The Hamiltonian for the Kondo model (without a magnetic field) is defined as

$$H = H_{\text{cond}} - \mathbf{J}\mathbf{S} \cdot \mathbf{s}. \quad (1)$$

Here, the first term is the Hamiltonian of the non-interacting conduction electrons by themselves, and the second term describes the interaction of the impurity spin  $\mathbf{S}$  with the spin  $\mathbf{s}$  of electrons in its immediate vicinity.  $J$  is a constant that describes the strength of these interactions. In a magnetic field  $B$ , there is an additional term, making the final Hamiltonian

$$H = H_{\text{cond}} - \mathbf{J}\mathbf{S} \cdot \mathbf{s} + \frac{g_i \mu_B}{\hbar} B J_z, \quad (2)$$

where  $g_i$  is an experimentally-determined “g-factor,”  $\mu_B$  is a fundamental constant known as the Bohr magneton, and  $J_z$  is the component of  $\mathbf{J}$  in the direction of the magnetic field.

For the spin-boson model, we again start with the Hamiltonian:

$$H = \Delta S_x + g u S_z + H_{\text{bosons}}. \quad (3)$$

The first term describes the quantum-mechanical tunneling of the impurity spin between its up and down states;  $\Delta$  measures the tunneling rate. The second term describes the coupling of the impurity spin to the bosons surrounding it (called the bosonic bath). The bosons can be thought of as quantized lattice vibrations, in which case  $u$  is the displacement of the impurity due to these vibrations. So  $g$  describes the strength of the coupling between the impurity spin and the bosonic bath. The last term is the Hamiltonian of the non-interacting bosons by themselves. For the purposes of this model, this bosonic bath is fully characterized by its density of states  $N(\omega)$ , which specifies the number of bosons having frequency  $\omega$ . In this project, we assumed

$$N(\omega) \propto \omega^s, \tag{4}$$

where  $\omega$  is the frequency of each boson state, and  $N(\omega)$  is the number of bosons in that state. The parameter  $s$ , then, defines the distribution of frequencies present in the bosonic bath.

Given the Hamiltonian, we can, in principle, solve for the possible quantum-mechanical energy states of the system. But in practice there is no way to solve this problem exactly, so we must come up with some way to approximate the answer. The NRG method, described in the next section, provides a way to accomplish this.

## 2.2 NRG Method

The numerical renormalization group (NRG) method is a powerful tool for solving magnetic impurity problems pioneered by Wilson [1] in the mid-70s. The basic idea behind the method is to break up a complex problem involving many length or energy scales into smaller problems (each involving a small section of the entire length or energy range) that can be solved in succession to arrive at an eventual answer. As might be expected with such a numerical method, the accuracy of the final answer can be increased either by partitioning into smaller bits or by looking at a larger total range of length or energy (both of which increase the necessary computing time).

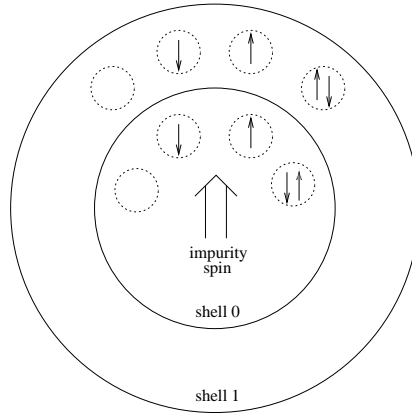


Figure 1: Shells representing successive iterations of the NRG calculation for the Kondo model. Each shell can hold zero electrons, one spin up electron, one spin down electron, or both a spin up and spin down electron.

The NRG method for the Kondo model can be pictured as in Fig. 1. First, we focus on a single impurity spin and the area in its immediate vicinity; imagine a shell around the impurity, just big enough to hold one electronic state. The Pauli exclusion principle tells us that only one fermion can reside in a single quantum mechanical state, or two if the fermions can have spin up or down. Therefore, the possibilities we need to consider inside the first shell are one spin up, one spin down, both, or neither. Since the impurity spin can be up or down, the first shell has a total of  $4 \times 2 = 8$  possible states.

It is possible to calculate physical properties of the system at this stage by calculating the energy levels of each of the eight possible states of the system. But this would be a very rough approximation, because we have not considered electrons traveling outside the first shell to other parts of the system. So we start adding shells, each time allowing for all the possible combinations of fermions filling each shell. By calculating the energy of each possible state of the combined system of multiple shells, we can use this information to determine the physical properties of the system. For example, in the first part of the project, we used a program that translates the energy levels from the NRG code into a plot of the specific heat as a function of temperature.

The number of states increases so quickly, however (with each shell the number of possible states is

multiplied by four, in this example), that we must limit the number of states kept at each iteration to some maximum  $k$ . Since we are generally interested in the low-energy or low-temperature behavior, we can get a good approximation by keeping the lowest  $k$  states.

As more shells are added, the approximation becomes better and better. Eventually, the energy levels settle toward their final values, at which time we can stop and use these values in our calculations. One way to look at this data is by plotting the energies of all the levels of the system versus the iteration number (i.e., how many shells have been added). Also called the NRG flow diagram, this type of plot shows how adding more shells affects the energy levels, which will be important when we study the quantum critical point.

The NRG method for the spin-boson model [2] is similar to that for the Kondo model, but here we consider bosons instead of fermions. Since bosons do not obey the exclusion principle, there could be any number of bosons inside each shell; but we must limit the number to some finite value so the calculation can be performed in finite time.

The accuracy of the NRG code's output can be controlled in a number of ways, which are accessible via a few parameters. For the spin-boson model,  $N_B$  defines the maximum number of bosons allowed in each shell, and a higher number will give better results. For both models we can vary  $k$  and  $\Lambda$ . The number of states kept after each iteration,  $k$ , is described above, and higher values produce better results.  $\Lambda$  is called the discretization parameter, and is used to specify the size of each shell. Specifically, the radius of the  $n$ th shell is defined as  $R_0\Lambda^n$ , where  $R_0$  is the radius of the first ( $n = 0$ ) shell. We are trying to approximate the case where the radius of each shell is only infinitesimally larger than the last one, in which case  $\Lambda$  would be arbitrarily close to 1. So lower values of  $\Lambda$  give better results, but we must set  $\Lambda$  higher than 1 to be able to run the calculation. There is, of course, a tradeoff; changing any of these parameters to produce more accurate results can significantly increase the necessary computing time.

## 2.3 Quantum Critical Points

When using the renormalization group method, certain parameters are said to “renormalize” to different values as the process advances. In the spin-boson model, for example, the coupling  $g$  of the bosons to the impurity spin generally renormalizes to either 0 or infinity. This terminology simply means that, for some values of  $g$ , the process of adding more shells in the NRG method decreases the effective value of  $g$  until it reaches 0, and for other values of  $g$ , the effective  $g$  increases until the behavior approaches that of  $g = \infty$ . In fact, in the spin-boson model, it is found that there is a critical value of  $g = g_c$  above which  $g$  renormalizes to  $\infty$  and below which it renormalizes to 0. This behavior is represented in Fig. 2.

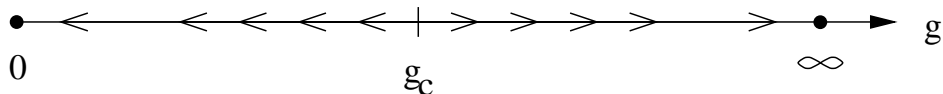


Figure 2: Schematic portrayal of the renormalization behavior of  $g$  in the spin-boson model.

The critical coupling  $g_c$  marks a critical point, the position of a phase transition between two different phases of the system. Furthermore, since the transition takes place at zero temperature and is controlled by a parameter other than the temperature, this is a *quantum* phase transition.

In this section of the project, the goal was to find the “critical exponents” characterizing the quantum phase transition in the spin-boson model. For phase transitions in general, we often see power-law behavior near critical points; this means that some physical quantities tend to be proportional to a distance from the critical point raised to some power, called the critical exponent. The quantum critical point of the spin-boson model occurs at  $g = g_c$ , temperature  $T = 0$ , and magnetic field  $B = 0$ ; hence, the critical exponents describe powers of  $|g - g_c|$ ,  $T$ , and  $|B|$ .

Finding the critical exponents, then, first requires that we know  $g_c$ . So the first step in my research was producing an algorithm that could find  $g_c$ , after which I could calculate the critical exponents.

Recent work described by Bulla et al. [2] claimed that the crossover temperature  $T^*$  (to be described

later) showed power-law behavior near the critical point, and critical exponents had been calculated for many values of  $s$ , the bath parameter. I aimed to reproduce these results to ensure that the code was working correctly, and then to move on to find critical exponents for other (mainly magnetic) properties.

### 3 $\text{Ce}_{0.6}\text{La}_{0.4}\text{Pb}_3$

#### 3.1 Tuning the Model

$\text{Ce}_x\text{La}_{1-x}\text{Pb}_3$  is a heavy-fermion system notable for its display of a single-impurity-like Kondo effect over a wide range of Ce concentration ( $0 < x < 0.96$ ). In particular, the Ce contribution to the specific heat at zero magnetic field seems to be linear in  $x$ .

Pietri [3] measured the low-temperature specific heat ( $C$ ) of  $\text{Ce}_{0.6}\text{La}_{0.4}\text{Pb}_3$  in magnetic fields and determined the part of the specific heat attributable to the impurity atoms (see Fig. 3). The goal in this section of my project was to see if the simple  $S = 1/2$  single-impurity Kondo model could account for the interesting properties that  $\text{Ce}_x\text{La}_{1-x}\text{Pb}_3$  displays at low temperatures in a magnetic field. Specifically of interest were the peaks in the specific heat curves.

To study  $\text{Ce}_x\text{La}_{1-x}\text{Pb}_3$  theoretically, we focus on the  $\text{Ce}^{3+}$ , which has an unpaired electron in its 4f shell. This electron can occupy one of six states of total angular momentum  $j = 5/2$ . Due to the electrostatic fields set up by the other atoms surrounding the Ce atom, these six states are split into a low-lying doublet and a higher-energy quartet sitting at an energy  $\Delta$  above. Experimentally,  $\Delta/k_B \simeq 77$  K, so at temperatures  $T \ll 77$  K, it is a good approximation to assume that only the doublet states will be occupied. This assumption allows one to map  $\text{Ce}^{3+}$  onto a spin 1/2 impurity.

When a magnetic field  $B$  is applied to a spin 1/2 impurity, the two impurity states (up and down) will split due to the Zeeman effect, with an energy difference given by

$$\Delta E = g_i \mu_B B. \tag{5}$$



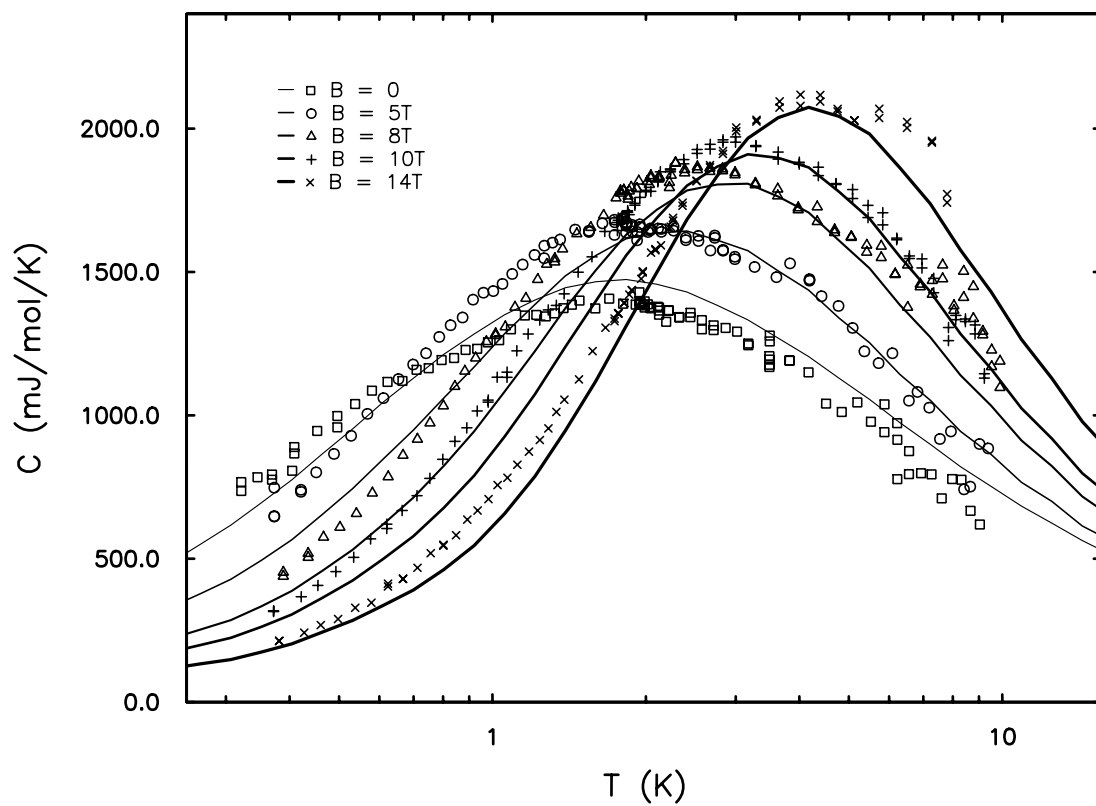


Figure 3: Experimental data from [3] (plotted as symbols) with single-impurity Kondo model data (plotted as curves;  $T_K = 2.6\text{ K}$ ) from the NRG code.

Here  $\mu_B$  is the Bohr magneton, and the  $g$ -factor  $g_i$  must be determined experimentally.

Application of a magnetic field to  $\text{Ce}^{3+}$ , on the other hand, produces a more complicated effect, because the field can cause the doublet and quartet states to mix. In the end, there is still a low-lying pair of states, but their energy splitting is not simply linear in  $B$ .

In the past (see, for example, Ref. [3]), this field-mixing of  $\text{Ce}^{3+}$  levels was ignored, and the splitting of the low-lying doublet was assumed to obey Eq. (5) with a constant  $g$ -factor,  $g_i = 10/7$ . In our research, however, we did not make this assumption, and instead calculated the energy levels of the quartet and doublet states for each value of the magnetic field, and hence determined the splitting  $\Delta E$ . We then used Eq. (5) to find an effective (field-dependent)  $g$ -factor  $g_i$  for use in the Kondo model.

### 3.2 Varying $T_K$

Our calculations contained one adjustable parameter: the Kondo temperature  $T_K$ . This theoretical parameter [which depends on  $J$  in Eq. (2) as well as the details of the conduction band] defines the characteristic temperature scale at which the Kondo effect appears in the material. The value cannot be determined *a priori*, however, so it was necessary to vary  $T_K$  in our model and search for the best fit. We tried  $T_K$  values from 2.0 to 3.0 K, plotting  $C$  vs.  $T$  for each value. Eventually we settled on  $T_K = 2.6$  K as the best match—the model data are plotted as curves in Fig. 3.

### 3.3 Results

We found the theoretical curves to agree well with the experimental data. The agreement is especially good around the peaks in  $C$ ; the locations and heights of the peaks agree well. Agreement at low and high temperatures was not as complete. However, the experimental error bars were also largest in these areas [3]; at temperatures below 1 K, the thermometry becomes less reliable, while above 10 K the electronic contribution to the specific heat tends to be swamped by the contribution from lattice vibrations.

We also tried fitting the experimental data using the model with a constant value of  $g_i = 10/7$  (regardless of the magnetic field, as described above) to see if the good agreement would persist with this assumption. We found that we were not able to fit as well in this case for any value of  $T_K$ . This result suggests that solving for the energy level splitting for each value of the magnetic field is a productive and necessary step.

## 4 Quantum Critical Points

### 4.1 Finding $g_c$

Using the NRG code to implement the spin-boson model, my first goal in this part of the project was to create an algorithm to find the critical coupling  $g_c$ . This goal was achievable because there are notable differences in the NRG flow of the energy levels among the  $g < g_c$ ,  $g > g_c$ , and  $g = g_c$  cases. Specifically, the flow of the first excited state can be used as an indicator of whether  $g$  is above or below the critical value. As illustrated in Fig. 4(a) and (b), for  $g < g_c$  the first excited state rises to a high final value, and for  $g > g_c$  it falls to a low final value. Closer to  $g_c$ , the unstable critical point emerges as a plateau at an intermediate energy [see Fig. 4(c)-(e)].

With this information, finding  $g_c$  is straightforward, at least in principle. Other complications arise, as explained later, but the basic algorithm is as follows:

1. Run the NRG code for  $g \gg g_c$  (i.e., 10) and  $g \ll g_c$  (i.e., 0) in order to find the energy that the first excited level reaches in the high- $g$  and low- $g$  limits.
2. Use these energy levels to establish threshold values. For example, the low- $g$  threshold might be set at 10% below the energy reached in the low- $g$  limit. Then, when another  $g$  value is tested, if the energy level goes above this threshold, we know the new  $g$  value must be below  $g_c$ .
3. Start at an intermediate value for  $g$  and, using the thresholds from step 2, determine if it is above or below  $g_c$ . Use this information to determine the next  $g$  value that should be tested, bisecting the

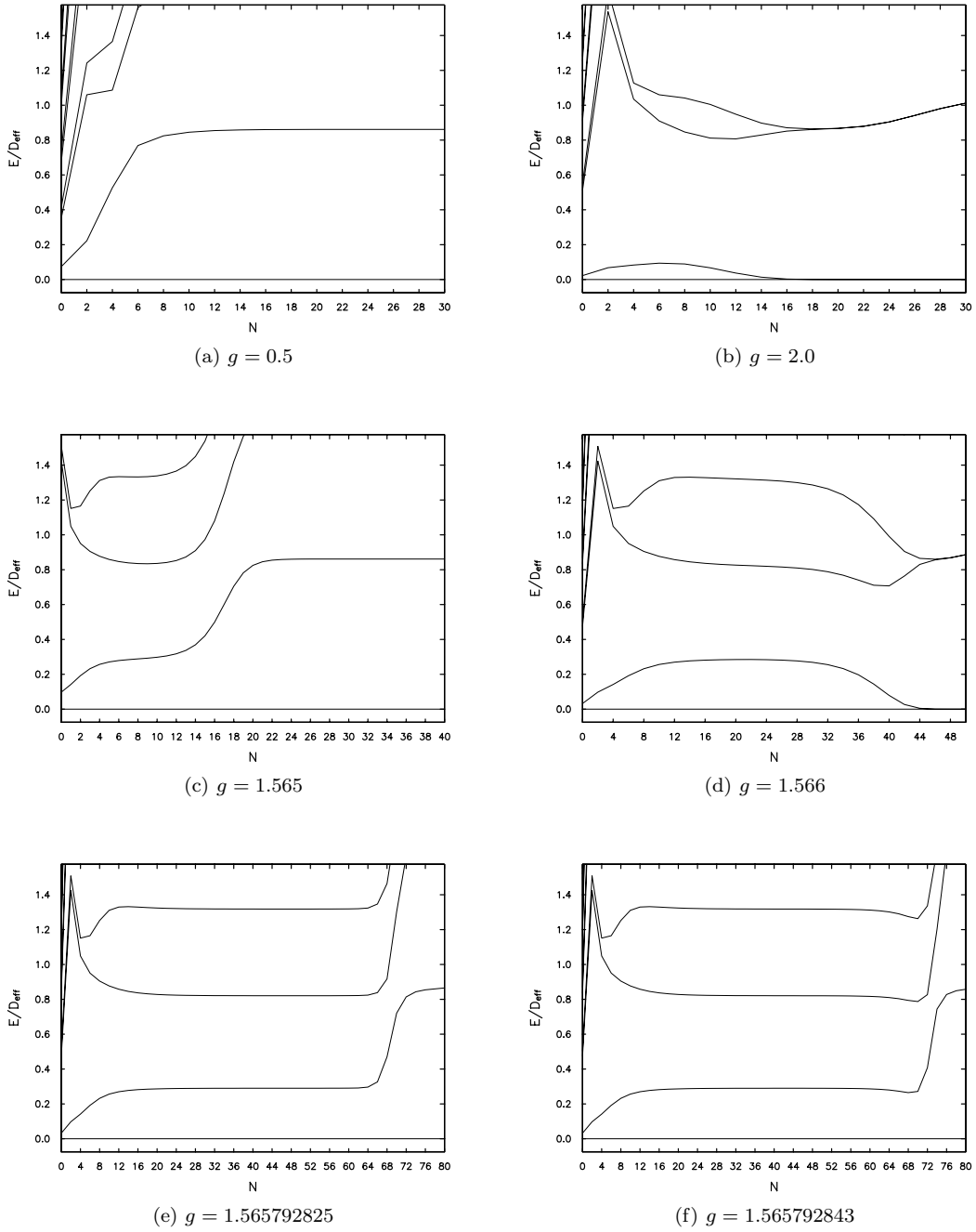


Figure 4: NRG flow diagrams for  $\Lambda = 3$ ,  $s = 0.8$ ,  $\Delta = 0.1$ , and varying coupling  $g$  progressively closer to  $g_c$ . In each case, in the plot on the left  $g < g_c$ ; on the right  $g > g_c$ . In (a) and (b), far from  $g_c$ , increasing the number of shells  $N$  causes the energy levels to quickly renormalize to  $g = 0$  and  $g = \infty$  limits, as is evident by looking at their first excited energy levels. In (c) and (d), the unstable critical state is seen before going to one or the other stable limit. In (e) and (f), numerical instabilities force the levels to the low- $g$  limit in both cases, but a dip in the first excited state in (f) allows us to see that it was heading for the high- $g$  limit.

interval in which  $g_c$  may lie.

4. Repeat step 3, always narrowing the range within which  $g_c$  is known to lie, until  $g_c$  is found (or, in practice, we reach a limit on determining  $g_c$  with any more precision).

The precision with which we can know  $g_c$  is limited by numerical instabilities that develop in the code due to rounding errors. The limiting instability in our runs presented itself in the following way. When  $g \approx g_c$ , the level is expected to rise to the critical energy, but eventually become unstable (since we are never *exactly* at  $g = g_c$ ) and either drop toward high- $g$  behavior or rise toward low- $g$  behavior [see Fig. 4(c) and (d)]. Numerical instabilities, however, cause the level to eventually rise sharply to low- $g$  behavior whether  $g$  is above or below  $g_c$  [see Fig. 4(e) and (f)]. The only chance, then, for determining if  $g > g_c$  is to find a slight dip in the energy before the numerical instability appears. To account for this, the code has an additional test for a slight dip after a long period of flatness. The code is also set up to be able to determine that, due to these instabilities, it is uncertain whether  $g$  is above or below  $g_c$ . In this case, we can go no further in narrowing our bounds on  $g_c$ .

The resulting output, then, is a range within which we know resides the critical coupling  $g_c$ . This code was run for values of the bath exponent  $s$  between 0.1 and 0.95, and values of the tunneling constant  $\Delta$  between  $10^{-1}$  and  $10^{-9}$ . These data, presented in Table I, were taken for  $\Lambda = 2$ ,  $N_B = 8$ ,  $k = 100$ , a combination of parameters that was found to produce accurate results while using a reasonable amount of computer time.

## 4.2 Finding critical exponents

Once the value of  $g_c$  is calculated for a certain set of parameters, one can find critical exponents that describe how properties change as  $g$  is varied close to the quantum phase transition. Following [2], we first looked at a temperature  $T^*$  that describes the scale at which the crossover occurs from the critical ( $T \gtrsim T^*$ ) to the stable ( $T \lesssim T^*$ ) fixed point. Referring back to Fig. 2, if we start with  $g$  slightly higher than  $g_c$ , it will

Table I: Critical coupling ranges calculated by the method described in the text for  $\Lambda = 2$ ,  $N_B = 8$ ,  $k = 100$ .

$s$	$\Delta$	$g_c$ min	$g_c$ max	$s$	$\Delta$	$g_c$ min	$g_c$ max
0.95	$10^{-1}$	2.983971834182	2.984004020691	0.4	$10^{-5}$	0.031287290039	0.031287295279
0.9	$10^{-1}$	2.385264486074	2.385265827179	0.4	$10^{-6}$	0.015789275639	0.015789291356
0.8	$10^{-1}$	1.714062423995	1.714062451907	0.4	$10^{-7}$	0.007974580221	0.007974588080
0.8	$10^{-2}$	1.071263425658	1.071263467525	0.4	$10^{-8}$	0.004028542898	0.004028584809
0.8	$10^{-3}$	0.744409963666	0.744410047401	0.4	$10^{-9}$	0.002035256475	0.002035298385
0.8	$10^{-4}$	0.547807275287	0.547807498783	0.3	$10^{-1}$	0.438976436853	0.438976455480
0.8	$10^{-5}$	0.416086525656	0.416086651385	0.3	$10^{-2}$	0.176211427897	0.176211441868
0.8	$10^{-6}$	0.321828462183	0.321829468012	0.3	$10^{-3}$	0.076796282082	0.076796313515
0.8	$10^{-7}$	0.251634120941	0.251641273499	0.3	$10^{-4}$	0.034384466707	0.034384482424
0.8	$10^{-8}$	0.198051333427	0.198056697846	0.3	$10^{-5}$	0.015512394020	0.015512417595
0.8	$10^{-9}$	0.156515054404	0.156524106861	0.3	$10^{-6}$	0.007013510912	0.007013594732
0.7	$10^{-1}$	1.300043720984	1.300043721476	0.3	$10^{-7}$	0.003173090517	0.003173202277
0.7	$10^{-2}$	0.740244732878	0.740244733534	0.3	$10^{-8}$	0.001435902668	0.001435913146
0.7	$10^{-3}$	0.471138474531	0.471138481517	0.3	$10^{-9}$	0.000649839639	0.000649895520
0.7	$10^{-4}$	0.317078552907	0.317078563385	0.2	$10^{-1}$	0.308796862513	0.308797532395
0.7	$10^{-5}$	0.219216179102	0.219216226251	0.2	$10^{-2}$	0.113384331614	0.113385085231
0.7	$10^{-6}$	0.153556894510	0.153556978331	0.2	$10^{-3}$	0.044696857668	0.044697192609
0.7	$10^{-7}$	0.108262300491	0.108262896538	0.2	$10^{-4}$	0.018013359069	0.018013925552
0.7	$10^{-8}$	0.076574236154	0.076576247812	0.2	$10^{-5}$	0.007306933403	0.007307529450
0.7	$10^{-9}$	0.054249763488	0.054253786803	0.2	$10^{-6}$	0.002971105277	0.002971440554
0.6	$10^{-1}$	1.002987897267	1.002987897558	0.2	$10^{-7}$	0.001209490001	0.001209657640
0.6	$10^{-2}$	0.523417518664	0.523417519100	0.2	$10^{-8}$	0.000492595136	0.000492930413
0.6	$10^{-3}$	0.304789622034	0.304789623197	0.2	$10^{-9}$	0.000200644135	0.000200867653
0.6	$10^{-4}$	0.186493296918	0.186493298228	0.1	$10^{-1}$	0.188808441162	0.188937187195
0.6	$10^{-5}$	0.116463117301	0.116463131272	0.1	$10^{-2}$	0.063743591308	0.063781738282
0.6	$10^{-6}$	0.073331330786	0.073331336026	0.1	$10^{-3}$	0.022917985916	0.022950172425
0.6	$10^{-7}$	0.046325748553	0.046325795702	0.1	$10^{-4}$	0.008411407470	0.008425712586
0.6	$10^{-8}$	0.029303729534	0.029304623604	0.1	$10^{-5}$	0.003097355365	0.003105401993
0.6	$10^{-9}$	0.018546953797	0.018547456712	0.1	$10^{-6}$	0.001145415008	0.001148432494
0.5	$10^{-1}$	0.774286166779	0.774286166862	0.1	$10^{-7}$	0.000425279140	0.000427961350
0.5	$10^{-2}$	0.370686978567	0.370686978786	0.1	$10^{-8}$	0.000157952308	0.000159293414
0.5	$10^{-3}$	0.196710143063	0.196710143937	0.1	$10^{-9}$	0.000058412551	0.000059604645
0.5	$10^{-4}$	0.108807370306	0.108807370798	0.05	$10^{-1}$	0.125732421875	0.126953125000
0.5	$10^{-5}$	0.061065896297	0.061065900227	0.05	$10^{-2}$	0.041427612304	0.042114257813
0.5	$10^{-6}$	0.034437739232	0.034437741852	0.05	$10^{-3}$	0.014438629150	0.014696121216
0.5	$10^{-7}$	0.019451403059	0.019451417029	0.05	$10^{-4}$	0.005187988281	0.005264282227
0.5	$10^{-8}$	0.010992215247	0.010992230964	0.05	$10^{-5}$	0.001850128173	0.001893043519
0.5	$10^{-9}$	0.006212815642	0.006213039160	0.05	$10^{-6}$	0.000658035278	0.000679492951
0.4	$10^{-1}$	0.590803736792	0.590803738100	0.05	$10^{-7}$	0.000237226486	0.000247955323
0.4	$10^{-2}$	0.259196100523	0.259196102268	0.05	$10^{-8}$	0.000084638595	0.000090003014
0.4	$10^{-3}$	0.124836369545	0.124836371507	0.05	$10^{-9}$	0.000030696392	0.000032037497
0.4	$10^{-4}$	0.062178384687	0.062178389344				

eventually renormalize to  $\infty$  as iterations of the NRG method are performed. If we start a little closer to  $g_c$ , it will still eventually renormalize to  $\infty$ , but this will require more iterations. Now imagine setting some threshold for the renormalized value of  $g$ —we will record the number of iterations ( $N^*$ ) required to reach that threshold for each starting value of  $g$ . We find that  $N^*$  increases as  $g$  gets closer to  $g_c$ .

This is essentially what we did to calculate the crossover energy  $T^*$ . To get from  $N^*$  to  $T^*$ , we used the fact that  $T$  is proportional to  $\Lambda^{-N}$  (as we get further from the impurity, the temperatures/energies we are dealing with are smaller and smaller). And since we could not directly set a threshold for the renormalized value of  $g$ , we instead set a threshold for the first excited energy level in the NRG flow. So for  $g < g_c$ , to find  $T^*$  for a certain value of  $g$ , we simply let the code run for that value until the energy of the first excited level rose above the predetermined threshold. In our runs, this threshold was generally set halfway between the low- $g$  energy and the critical  $g$  energy. We called the first iteration at which the energy is above the threshold  $N^*$  (we also performed a linear interpolation so we were not limited to discrete values of  $N^*$ ).

We were expecting [2] a relationship of the form

$$T^* \propto |g_c - g|^{\nu z}, \quad (6)$$

so we plotted  $T^*$  versus  $|g_c - g|$  on a log-log plot. The slope of the resulting line was the critical exponent  $\nu z$ . An example of such a plot is given in Fig. 5.

To find the critical exponent for a given bath parameter  $s$  [see Eq. (4)], the slope of this line was found by making a least-squares fit over a range of  $|g_c - g|$  that is well-approximated by such a power-law fit. Our data are presented in Fig. 6. We used  $s$  values between 0.1 and 0.95. The data are in qualitative agreement with the analogous figure in Ref. [2], and seem to be in quantitative agreement except for the  $s = 0.1$  point, which is significantly higher in our calculations.

We were also interested to know how these critical exponents are affected by changing the maximum number of bosons in each shell ( $N_B$ ) and the number of states kept at each iteration ( $k$ ). Increasing either

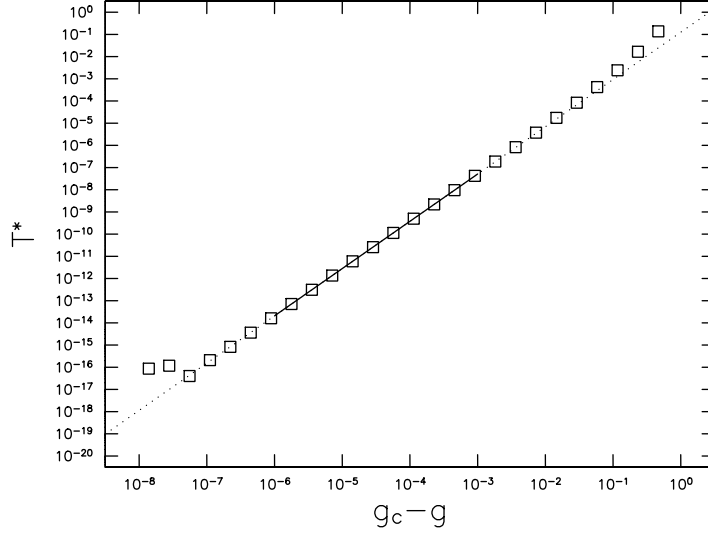


Figure 5: A sample  $T^*$  versus  $(g_c - g)$  plot (for  $g < g_c$ ,  $s = 0.8$ ,  $\Delta = 0.1$ ). The fit line is solid through the points used to find the least-squares fit, dotted otherwise. The slope of this line gives the critical exponent, and corresponds to the  $s = 0.8$  point on Figure 6.

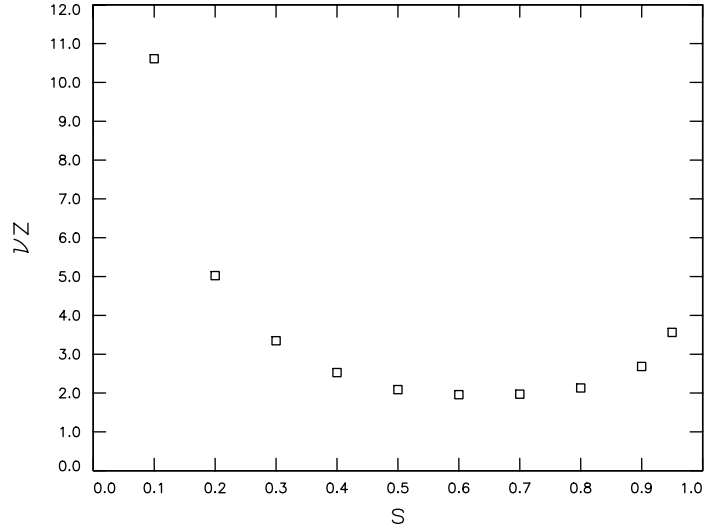


Figure 6: The  $T^*$  critical exponents for  $g < g_c$ ,  $\Lambda = 2$ ,  $N_B = 8$ ,  $k = 100$ , and varying bath exponent  $s$  in the spin-boson model.



of these parameters increases the accuracy of the calculation, but it also increases the computer time. To find the minimum values needed for an accurate result, I calculated critical exponents for  $4 \leq N_B \leq 15$  and  $50 \leq k \leq 200$ , and determined the values above which the critical exponents did not change significantly. The values  $N_B = 8$ ,  $k = 100$  were determined to be sufficient, and were therefore used for most of our calculations. I also tested  $\Lambda = 3$ , which did not produce significant change in the critical exponents.

Finally, we also wished to find critical exponents for  $g > g_c$ . In principle one should find the same values as for  $g < g_c$ . In this case, we test for the first iteration at which the first excited energy level drops *below* some threshold level. This case was complicated by the fact that, as discussed above, the level does not always drop all the way down to the high- $g$  limit, but can rise to the low- $g$  limit due to numerical instabilities. Due to this problem, the threshold level was not set halfway between the critical limit and the high- $g$  limit, but rather just below the critical limit. Still, most of the resulting critical exponents were, as expected, not significantly different than the  $g < g_c$  case. For low  $s$ , however, and especially for  $s = 0.1$ , the critical exponents were significantly below the  $g < g_c$  case. Initial tests with  $g < g_c$  suggest that changing the threshold level does cause the critical exponents to change at low  $s$ . It is possible that this is the reason for the discrepancy with the  $s = 0.1$  point between our data and that in Ref. [2].

## 5 Conclusion

The agreement of the Kondo model data to experimentally-gathered specific heat data suggests that much of the underlying physics of heavy-fermion systems is captured in the Kondo model, an interesting result considering the simplicity of the model. Our agreement with the critical exponent results for  $T^*$  in Ref. [2] indicates that our code is working correctly, and our work in calibrating this code opens the door for more in-depth study of the quantum phase transition. Unfortunately, time ran out before we could study the critical exponents of any other properties. With so much left to explore, the results of this project are likely to lead to future investigation that will reveal even more about heavy-fermion systems.

## Acknowledgements

I would like to thank specifically Prof. Kevin Ingersent, and in general the University of Florida Physics Department, for providing generous guidance and support. Funding for this research was provided by the National Science Foundation through the Research Experiences for Undergraduates program.

## References

- [1] K. G. Wilson, *Rev. Mod. Phys.* **47**, 773 (1975).
- [2] R. Bulla, N. H. Tong, and M. Vojta, *Phys. Rev. Lett.* **91**, 170601 (2003).
- [3] R. Pietri, *Magnetism and the Kondo effect in cerium heavy-fermion compounds: CeAl<sub>3</sub> and CePb<sub>3</sub>* (University of Florida Ph.D. dissertation, 2001).